

VR-GS: A Physical Dynamics-Aware Interactive Gaussian Splatting System in Virtual Reality

YING JIANG^{1,2*}, CHANG YU^{1*}, TIANYI XIE^{1*}, XUAN LI^{1*}, YUTAO FENG^{3,4}, HUAMIN WANG⁵, MINCHEN LI⁶, HENRY LAU², FENG GAO⁷, YIN YANG³, and CHENFANFU JIANG¹



Fig. 1. **Animal Crossing.** Utilizing our system, individuals can engage in intuitive and interactive physics-based game-play with deformable virtual animals and realistic environments represented with 3D Gaussian Splatting.

As consumer Virtual Reality (VR) and Mixed Reality (MR) technologies gain momentum, there’s a growing focus on the development of engagements with 3D virtual content. Unfortunately, traditional techniques for content creation, editing, and interaction within these virtual spaces are fraught with difficulties. They tend to be not only engineering-intensive but also require extensive expertise, which adds to the frustration and inefficiency in virtual object manipulation. Our proposed VR-GS system represents a leap forward in human-centered 3D content interaction, offering a seamless and intuitive user experience. By developing a physical dynamics-aware interactive Gaussian Splatting (GS) in a VR setting, and constructing a highly efficient two-level embedding strategy alongside deformable body simulations, VR-GS ensures real-time execution with highly realistic dynamic responses. The components of our VR system are designed for high efficiency and effectiveness, starting from detailed scene reconstruction and object segmentation, advancing through multi-view image in-painting, and extending to interactive physics-based editing. The system also incorporates real-time deformation embedding and dynamic shadow casting, ensuring a comprehensive and engaging virtual experience. Our project page is available at: <https://yingjiang96.github.io/VR-GS/>.

1 INTRODUCTION

The burgeoning growth in commercial VR and MR applications is propelling the quest for high-fidelity 3D content within the Computer Graphics (CG) and Computer Vision (CV) communities. Despite their capabilities of being rendered efficiently in VR, traditional 3D/4D content creation, reliant on 3D modeling tools and game engines, is time-intensive and complex, often beyond the reach of non-expert users. This accessibility barrier limits broader user engagement in high-quality content creation.

Recognizing the advantages and limitations of the traditional graphics pipeline, our goal is to find a modern variant. To enhance

the visual quality and ease of creation for non-expert users, we move away from traditional 3D models in graphics pipelines and instead, adopt state-of-the-art radiance field techniques for rendering. In this context, Neural Radiance Fields (NeRF) emerge as a natural choice. Despite its versatility, NeRF’s volume rendering falls short in efficiency for interactive rendering on Extended Reality (XR) devices, which demand high frame rates. Additionally, NeRF’s approach to handling deformations—requiring bending of query rays via an inverse deformation map—is slow [43]. Fortunately, 3D Gaussian Splatting (GS) [17] has been recently introduced as an efficient and explicit alternative to NeRF. This method not only excels in rendering efficiency but also provides an explicit geometric representation that can be directly deformed or edited. The explicit nature of 3D GS can simplify the direct manipulation of geometry by solving a Partial Differential Equation (PDE) that governs the motions of Gaussian kernels. Furthermore, GS eliminates the need for high-fidelity meshes, UV maps, and textures, offering the potential for naturally photorealistic appearances. It is worth noting that many studies have already demonstrated the use of 3D GS for 4D dynamics [41, 43, 64] and the integration of physics-based simulations for more realistic 4D content generation [9, 60], as well as for creating animatable avatars [63, 68].

In this paper, we introduce VR-GS, a physics-aware, interactive Virtual Reality (VR) system for immersive manipulation of 3D content represented with Gaussian Splatting (GS). To ensure an interactive experience, we utilize eXtended Position-based Dynamics (XPBD) [32], a highly adaptable and unified physical simulator, for real-time deformation simulation. Direct incorporation of a simulator onto GS kernels presents challenges, as the simulation and rendering processes have distinct geometrical representations. To address this, we construct a tetrahedral cage for each segmented

* indicates equal contributions.

Affiliations: ¹UCLA, ²HKU, ³Utah, ⁴ZJU, ⁵Style3D Research, ⁶CMU, ⁷Amazon

GS kernel group and embed these kernel groups into corresponding meshes. The deformed mesh, driven by XPBD, subsequently guides the deformation of the GS kernels. Noticing that simplistic embedding techniques can lead to undesirable, spiky deformations in GS kernels, we propose a novel two-level embedding approach. This method allows each Gaussian kernel to adapt to a smoothed average deformation of the surrounding tetrahedra. The intricate combination of GS and XPBD through our two-level embedding not only achieves real-time physics-based dynamics but also upholds high-quality, realistic rendering, enabling high-fidelity immersive VR experiences. In summary, our contributions include:

- *Immersive VR System Development:* The development of a VR system blending physical dynamics with high-fidelity appearance for enriched user experiences. We extensively evaluate our framework with various experiments including user studies.
- *Real-Time 3D Content Interaction:* The engineering of the system with a focus on human-centric, creative interaction with captured and virtual 3D content.
- *Comprehensive System Integration:* The comprehensive combination of 3D GS, segmentation, image inpainting, and real-time physics-based solvers with a novel rendering geometry embedding algorithm.

2 RELATED WORK

2.1 Radiance Fields Rendering

A variety of 3D representations, such as mesh [50], point clouds [44], signed distance fields [57], and grids [67] were exploited in early work for visual computing tasks, including synthesis, estimation, manipulation, animation, reconstruction, and transmission of data about objects and scenes [11, 17, 61]. Since neural radiance fields (NeRF) [34] was proposed for novel view synthesis with differentiable volume rendering, it has been applied to versatile computer graphics and computer vision tasks, such as scene reconstruction [33, 39, 65], synthesis [14, 52], rendering [30, 59] and animation [3, 42], simulation [25], etc. While Neural Radiance Fields (NeRF) have achieved remarkable image quality, they suffer from significant time and memory inefficiencies [28]. To mitigate these issues, various methods have been introduced. Sparse representations [29], decomposed strategies [38, 46], and multi-resolution encoding [36] have all been proposed to enhance volume rendering efficiency while maintaining high quality. However, NeRFs are implicit representations, making it challenging to detect and resolve collisions [45]. Recently, 3D Gaussian splatting (GS) proposed by Kerbl et al. [17] utilizes an array of 3D Gaussian kernels to represent scenes explicitly, facilitating faster optimization and achieving state-of-the-art results.

2.2 Editing in Radiance-based Scene

A natural extension of NeRF is to support user-guided editing. Li and Pan [24] made use of two proxy cages to offer interactive control of the shape deformation of NeRF. Besides geometry editing, text prompts [56] or a user-edited image [2] can also be adopted to conduct style transfer of NeRF. Besides, Lin et al. [27] put forward

exploiting 2D sketches to edit high-quality facial NeRF. Concerning NeRF texture editing, Huang et al. [14] utilized a coarse-fine disentanglement representation and a patch-matching algorithm to synthesize textures of different shapes from multi-view images. What’s more, De-Nerf [59] exploits a hybrid light representation that enables users to relight NeRF. In contrast, Gaussian Splatting is more appropriate for post-editing tasks thanks to its explicit nature and inspired a series of follow-up works [4, 7, 8, 15, 66].

Another significant direction in NeRF research is the incorporation of dynamic details into static scenes. To achieve this, a popular strategy [41, 43] is to consider time as an additional input to the system. This method typically splits a dynamic NeRF into a canonical static field and a deformation field, with the latter mapping this canonical representation to a deformed one. More recently, Yang et al. [64] drew inspiration from 3D GS to reconstruct a dynamic scene using 4D Gaussian primitives that change over time. However, the dynamics in these methods are generally confined to motions captured from input data, limiting their ability to synthesize unseen dynamics. To generate novel dynamics, Xie et al. [60] and Feng et al. [9] have integrated physics-based simulations into 3D static representations, paving the way for generating physically plausible and novel dynamic scenes.

2.3 Neural Radiance Fields in VR

Rendering NeRF is computationally expensive for real-time VR applications, which causes high latency and low quality [21, 49]. To address these challenges and enable high-fidelity rendering with minimal latency on a single GPU, various techniques have been proposed. These include gaze-contingent 3D neural representations [6], variable rate shading [47], and hybrid surface-volume representations [55], all aimed at accelerating NeRF. In contrast, VR-NeRF [62] leverages multiple GPUs to achieve high-quality volumetric rendering of NeRF. Beyond software acceleration techniques, RT-NeRF [19] utilizes an algorithm-hardware co-design framework to provide real-time NeRF solutions for immersive VR rendering. While these methods primarily focus on enhancing NeRF rendering, our work is dedicated to facilitating interactive editing within a VR environment.

Li et al. [22] integrated affine transformation with NeRF to enable interactive features, such as exocentric manipulation, editing, and VR tunneling effects. However, their approach is limited to filter-based edits such as edge blurring and fails to support the deformation of virtual objects’ geometry. RealityGit [20] and Magic NeRF Lens [23] modify a NeRF model by erasing or revealing a portion of NeRF. Nevertheless, neither system possesses the functionality to deform the geometrical structure of the model as well. In contrast to these works which concentrate on interactive editing of NeRF, our paper introduces VR-GS, a new physical dynamics-aware interactive system for GS in VR, first enabling users to interact with 3D GS at a real-time rate.

3 DESIGN GOALS AND DESIGN DECISIONS

We propose the development of a unified, physics dynamics-aware interactive VR system, meticulously designed for real-time interaction with Gaussian Splatting (GS).

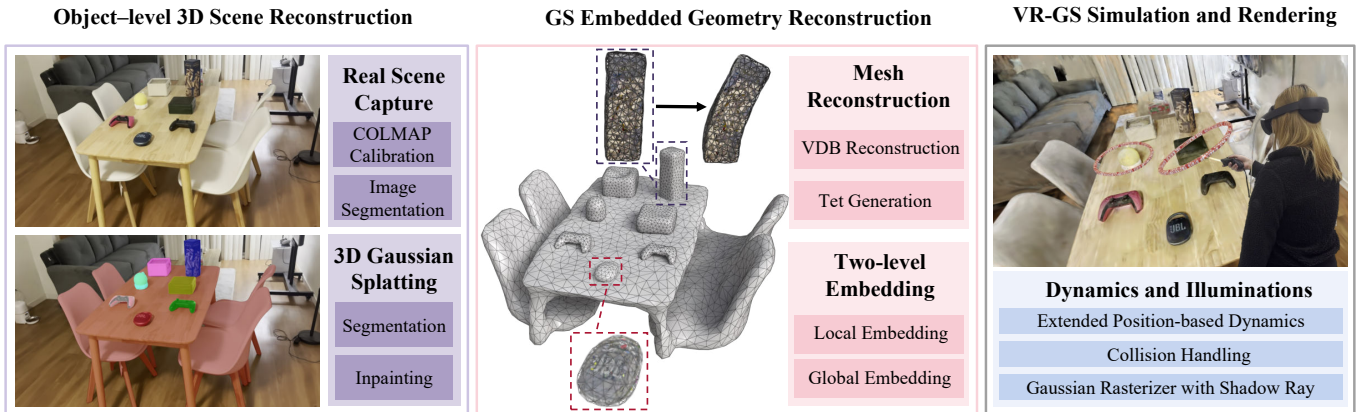


Fig. 2. VR-GS is an interactive system meticulously crafted to integrate 3D Gaussian Splatting (GS) and eXtended Position-based Dynamics (XPBD) for generating a real-time interactive experience in Virtual Reality (VR). Beginning with multi-view images, the pipeline skillfully combines scene reconstruction, segmentation, and inpainting using Gaussian kernels. These kernels form the foundation for VR-GS’s utilization of the sparse volumetric data structure VDB, facilitating bounding mesh reconstruction and subsequent tetrahedralization. VR-GS further harnesses a novel two-level rendering geometry embedding, XPBD, collision detection, and shadow casting techniques, all converging to deliver a captivating and immersive user experience.

3.1 Design Goals

G1. Immersive and Realistic. A VR system should provide a deeply immersive 3D environment that convincingly simulates physical presence, where objects possess a high degree of realism [16]. Accordingly, our targeted VR system aims to offer users an experience that is both immersive and realistic, characterized by dynamic motions, 3D virtual shapes, and illuminations that closely mirror the real world. This goal sets our system apart, especially in how it handles physics-based 3D deformations and dynamics, as opposed to those that rely solely on geometric deformation.

G2. Real-Time Interaction. For a VR system, low latency is crucial to prevent disorientation or motion sickness [6, 53]. Slow system responses can severely impair the quality of interaction. Our proposed VR system is engineered to provide users with instantaneous output and feedback during their interaction. This includes real-time responsiveness in various operations such as transformation, rotation, scaling, duplication, undoing, as well as physical and geometric editing. To our knowledge, VR-GS represents the first interactive physics-based GS editor.

G3. Unified Framework. VR-GS exemplifies a holistic framework, skillfully integrating both rendering and simulation within a single unified system. Our design philosophy focuses on harmonizing various 3D representation formats, utilizing a blend of thoughtful algorithms and design principles. This integrated approach guarantees a seamless user experience, adhering to the concept of “what you see is what you simulate”[35].

G4. User-Centric Design. Essential to a user-friendly VR system is the integration of a flexible model or simulation that supports intuitive and task-oriented user interaction [51]. VR-GS is designed to provide this intuitive control, along with responsive feedback, ensuring a natural and seamless interaction experience. The system’s

operations and outputs are meticulously aligned with user expectations and commonsense understandings [10, 12]. Furthermore, VR-GS’s scene in-painting capability, which effectively fills gaps resulting from object removal, is a testament to its commitment to meeting user expectations.

3.2 Design Decisions

Our design decisions align closely with the design goals.

D1. Physics-Based Generative Dynamics. The VR-GS system leverages physics-based simulation techniques to produce realistic dynamics and facilitate 3D shape editing. Unlike methods that reconstruct motion from time-dependent datasets or utilize generative AI to drive Gaussian models, our system adheres to physical principles.

D2. Real-Time Editing and Manipulation. To achieve both real-time performance and physically realistic editing and manipulation, we implement a reduced representation model and parallel-friendly algorithms within our frame budget. While the per-Gaussian-based discretization as done in [60] offers detailed dynamics, its time cost is impractical for our system’s needs. Instead, we utilize a tetrahedral mesh embedding reconstructed from Gaussian kernels to drive GS motion. We adopt XPBD with finite-element constraints to achieve real-time simulation paradigm prevalent in gaming and VR applications.

D3. Unified Simulation and Rendering. Our system employs a hybrid approach, combining cage mesh and Gaussian kernels, to achieve real-time performance. To enhance alignment between these two representations, we focus on integrating their functionalities. The deformation gradient field from the cage mesh is adept at embedding a volumeless point cloud. However, as each Gaussian kernel resembles a rotated ellipsoid, it can lead to spiky artifacts during large deformation, a challenge highlighted in [60]. To mitigate this, we employ a two-level interpolation strategy: initially embedding each Gaussian within an individual tetrahedron, followed by embedding

these tetrahedra within the cage mesh to elevate the smoothness of the deformation field.

D4. Natural User Control and Prepossession. Diverging from traditional 2D interface inputs, VR-GS harnesses 3D input mechanisms for interacting with 3D objects. Moreover, the system incorporates object segmentation and scene inpainting functionalities to seamlessly fill gaps created by object removal in the GS training process. This integration ensures a consistent and coherent user experience.

4 METHOD

4.1 Gaussian Splatting

Gaussian splatting, proposed by Kerbl et al. [17], is an explicit 3D representation to encapsulate 3D scene information using a set of 3D anisotropic Gaussian kernels, each with learnable mean μ , opacity σ , covariance matrix Σ , and spherical harmonic coefficients C . Spherical harmonics (SH) are expansions of the view-dependent color function defined on the unit sphere.

To render a view, the 3D splats are projected to 2D screen space ordered by their z -depth. The color C of a pixel is computed by α -blending of these 2D Gaussians from near to far:

$$C = \sum_{i \in N} c_i \alpha_i \prod_{j=1}^{i-1} (1 - \alpha_j), \quad (1)$$

where c_i is the evaluated color by SHs viewed from the camera to the kernel’s mean. α_j is the product of the kernel’s opacity and 2D Gaussian weight evaluated at the pixel coordinate. Leveraging a differentiable implementation, the rendering loss towards the ground truth image can be backpropagated to Gaussians’ parameters for optimization.

In contrast to traditional NeRFs based on implicit scene representations, GS provides an explicit representation that can be seamlessly integrated with post-processing manipulations, such as animating and editing. Moreover, the efficient rasterization and superior rendering quality of 3D Gaussians facilitate their integration with VR.

4.2 VR-GS Assets Preparation

Each 3D asset in our VR system consists of a high-fidelity 3D GS reconstruction and an enveloping simulatable tetrahedral mesh in a moderate resolution to enable real-time physics-aware dynamics. These preparations are conducted offline before immersive and interactive editings within our VR environment, which includes:

- *Segmented GS Generation:* we support interactions with individual objects in a large scene, achieved by segmented GS reconstructions.
- *Inpainting:* The occluded parts between the objects and their supporting planes usually have no texture. We inpaint 3D GS representations leveraging a 2D inpainting technique.
- *Mesh Generation:* A simulation-ready tetrahedral mesh is generated for each object.

Segmentation. The segmented GS is constructed during the GS reconstruction. We first generate 2D masks on the multi-view RGB images by utilizing a 2D segmentation model [5]. Each segmented part is assigned a different color that is consistent across different views. Subsequently, we enhance the scene representation by

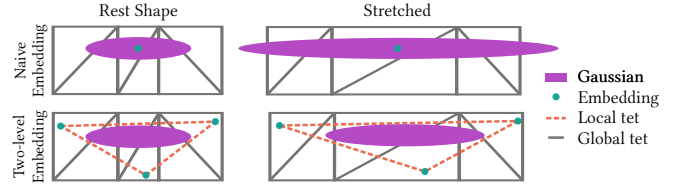


Fig. 3. Our two-level embedding effectively resolves spiky artifacts. Each Gaussian kernel is embedded into a local tetrahedron. The vertices of the local tetrahedron are independently embedded into the global mesh.

integrating three additional learnable RGB attributes into the 3D Gaussian kernels. During the reconstruction process, each 3D Gaussian kernel will automatically learn what object it belongs to utilizing a segmentation loss function L_{seg} :

$$L_{\text{seg}} = L_1(M_{2d}, I), \quad (2)$$

where M_{2d} represents colored 2D segmentation results and I denotes the rendering of 3D Gaussian kernels with colors replaced by the extended RGB attributes instead of evaluated from SHs. Thus, the total loss becomes

$$L_{\text{total}} = (1 - \lambda)L_1 + \lambda L_{\text{SSIM}} + \lambda_{\text{seg}} L_{\text{seg}}, \quad (3)$$

where L_1 and L_{SSIM} are computed between the normally rendered images and the multi-view ground truths. We use $\lambda = 0.2$ and $\lambda_{\text{seg}} = 0.1$ in all our experiments.

Inpainting. After 3D GS segmentation, we extract all objects separately from the scene. This process of object removal, however, results in the emergence of holes within the regions that are previously occluded. To alleviate the issue, we utilize 2D inpainting tool LaMa [54] to guide the 3D inpainting of Gaussian kernels. We freeze the Gaussian kernels located outside of the holes and then use an inpainting loss $L_{\text{inpaint}} = L_1(I_{\text{inpainted}}, I)$ to optimize a Gaussian kernel patch under the guidance of the 2D inpainted images $I_{\text{inpainted}}$ for the current 3D GS rendering I . The result of our inpainting is validated in Section 5.

Mesh Generation. Due to our design choice to use mesh-based simulation, we generate a tetrahedral mesh for each group for the segmented 3D Gaussian kernels. These meshes will not be rendered during the interaction but only serve as the media of dynamics. Hence, we do not require high-fidelity meshes, which, in return, boost the performance of our system. To construct a mesh, we first use internal filling proposed by [60] to fill particles into the void internal region, which failed to be reconstructed by GS. Then we treat centers of Gaussians as a point cloud and convert it to a voxel representation represented by the VDB format[37]. A water-tight surface mesh is extracted from this VDB using marching cubes [31], which is then served as the boundary of the volume to generate a simulation-ready tetrahedral mesh by TetGen [48].

4.3 Unified Framework for Simulation and Rendering

As derived in Xie et al. [60], Gaussian kernels can be deformed by the deformation map given by the simulation. We follow the Gaussian kinematics of this work but replace the simulation with

eXtended position-based dynamics (XPBD) [32] to achieve real-time interactions. We employ the strain energy constraint as the elastic model and adopt the velocity-based damping model in the XPBD framework. To resolve collisions between meshes in real-time, penalty forces based on point-triangle distance constraint are added on close triangles pairs detected by LBVH [40].

In mesh-based simulation, the deformation map is given by a piece-wise linear map, where the deformation gradient is hence constant within each tetrahedron. Given a tetrahedron with the rest-shape configuration $\{\mathbf{x}_0^0, \mathbf{x}_1^0, \mathbf{x}_2^0, \mathbf{x}_3^0\}$ and the current configuration $\{\mathbf{x}_0, \mathbf{x}_1, \mathbf{x}_2, \mathbf{x}_3\}$, the deformation gradient is defined as

$$F = [\mathbf{x}_1 - \mathbf{x}_0, \mathbf{x}_2 - \mathbf{x}_0, \mathbf{x}_3 - \mathbf{x}_0] [\mathbf{x}_1^0 - \mathbf{x}_0^0, \mathbf{x}_2^0 - \mathbf{x}_0^0, \mathbf{x}_3^0 - \mathbf{x}_0^0]^{-1}, \quad (4)$$

where the inverse of the rest-shape basis can be computed pre-simulation. The mean and the covariance matrix of the deformed Gaussian kernel inside this tetrahedron is given by

$$\boldsymbol{\mu} = \sum_i w_i \mathbf{x}_i, \quad \Sigma = F \Sigma_0 F^T, \quad (5)$$

where w_i is the barycentric coordinates of the initial center $\boldsymbol{\mu}_0$ in the rest-shape configuration, and Σ_0 is the initial covariance matrix [60]. The deformed Gaussian kernels can be directly rendered by the point splatting procedure. However, the direct embedding of Gaussian centers cannot guarantee that every ellipse shape is completely enveloped by some tetrahedron inside the simulation mesh. As shown in Figure 3, this can lead to spiky artifacts.

Observe that kernels that are completely inside the tetrahedron will always be inside. This motivates us to propose a two-level embedding procedure:

- Local embedding: we independently envelope every Gaussian kernel by an as-tight-as-possible tetrahedron. There is no connectivity between these local tetrahedra.
- Global embedding: we embed the vertices of local tetrahedra into the global simulation mesh.

As the global mesh is deformed by the simulation, the vertices of local tetrahedra are kept inside the boundary, driving the kinetic evolution of Gaussian kernels. A local tetrahedron could overlap with multiple global tetrahedra. The deformation map on it can be understood as the average of the surrounding global tetrahedra, hence eliminating sharp, spiky artifacts, as validated in Section 5.

Shadow Map. While the original global illumination of the scene can be accurately learned and baked by the spherical harmonics on each Gaussian, the shadow will no longer be aligned with the object when it is moving or deforming. The introduction of the shadow map [58] into the GS framework can enhance the immersive experience in VR. More importantly, it can guide human perception of the spatial relationships between objects: during manipulation, users will rely on the shadow to determine the distance between objects. The shadow map is a fast real-time algorithm and is well-aligned with the GS rasterization pipeline. We follow Equation (1) to estimate the depth map from the light source and test the visibility for each Gaussian using this depth map. The influence of shadow maps is ablated in Section 5.

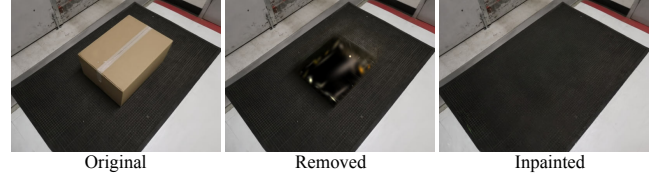
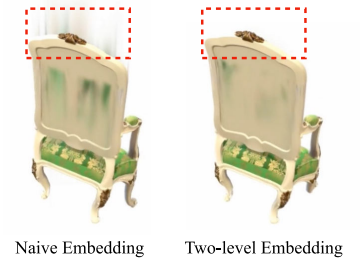


Fig. 4. **Inpainting Evaluation.** GS struggles to reconstruct occluded surfaces. By leveraging LAMA [54], we produce 2D inpainted results that guide the 3D scene inpainting, enhancing the realism of the 3D representation.

5 EVALUATION

In this section, we assess the essential components of our proposed system, including two-level GS embedding and shadow map.

Two-level Embedding. The two-level embedding is a crucial component in our physical dynamics-aware system, integrating the tetrahedra cage mesh with the embedded Gaussian. In the inset figure, we conduct an ablation study to validate the effectiveness of



our two-level embedding approach. Under conditions of extreme stretching or twisting, the naive embedding method, which merely embeds the Gaussian kernel within the closest tetrahedron, leads to severe spiky artifacts. Our two-level embedding strategy addresses this by initially embedding each Gaussian into a localized, independent tetrahedron, followed by embedding the vertices of this tetrahedron into the cage mesh. The deformation of each Gaussian kernel is determined by averaging the deformations at these vertices, resulting in a smoother deformation gradient field than the naive approach and significantly reducing spiky artifacts.

Inpainting. With the guidance of 2D segmentation image results, our system achieves object-level 3D scene reconstruction, facilitating convenient post-physics-based manipulation. However, GS is limited to reconstructing surfaces visible in the provided multi-view training images. Consequently, some object and background areas, unseen in these images, remain unreconstructed by GS, leading to 'black hole' like artifacts when foreground objects are moved. To address this, our system integrates the object segmentation mask with LAMA [54], a 2D inpainting model, to generate inpainted multi-view images. These images then guide the fine-tuning and inpainting of our 3D GS scene, yielding a more complete and realistic user experience, as evidenced in Figure 4.

Shadow Map. Furthermore, we take advantage of the shadow map to add extra time-dependent shadow into the GS scene, as shown in 5. Original GS models shadows as fixed surface textures, and thus fails to provide dynamic shadows as objects move around the scene. VR-GS allows users to choose the parameters, e.g. position and direction, of the light source to reproduce the lighting setting of the original scene, leading to a more realistic VR environment.

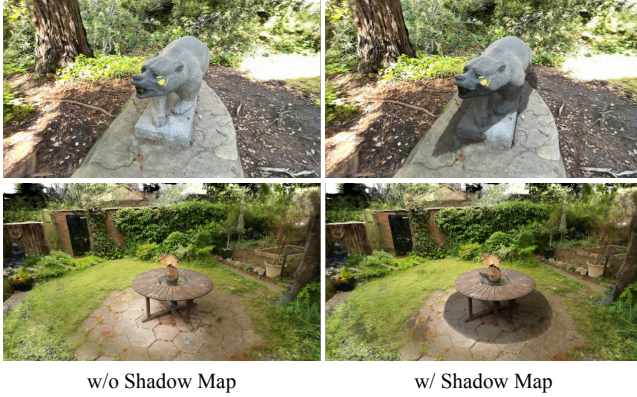


Fig. 5. **Shadow Map Evaluation.** GS traditionally models shadows as static surface textures. Our approach, employing a shadow map, generates dynamic shadows for a more immersive experience.

6 EXPERIMENT

In this section, we benchmark our VR-GS system’s simulation performance against other leading methods in GS and NeRF manipulation. Additionally, we present immersive and interactive demos within our VR-GS system. Our prototype, developed on Unity with a CUDA-implemented plugin, is tested using a Quest Pro Head-Mounted Display (HMD) and corresponding controllers, on a high-performance Intel(R) Core(TM) i9-14900KF CPU with 32GB memory and an NVIDIA GeForce RTX 4090 GPU.

6.1 Performance

We compared VR-GS against two state-of-the-art NeRF/GS physics-based manipulation methods: PAC-NeRF [25]

| Example | PAC-NeRF | Phys-Gaussian | VR-GS (Ours) |
|-----------|----------|---------------|--------------|
| Stool | 0.750 | 0.112 | 0.017 |
| Chair | 0.813 | 0.219 | 0.022 |
| Materials | 0.625 | 0.39 | 0.021 |

and PhysGaussian [60]. PAC-NeRF primarily concentrates on estimating material parameters from multi-view videos in reconstructed NeRF scenes. Although it offers novel dynamic generation capabilities, the resulting visuals often fall short in rendering quality. In contrast, PhysGaussian, leveraging GS, produces superior photorealistic dynamics. However, the Material Point Method (MPM) used by both systems can limit real-time performance in extensive scenes. For a fair comparison, we standardize the frame time ($\Delta t_{\text{frame}} = 1/25$ sec) and the simulation step time ($\Delta t_{\text{step}} = 0.0001$ sec) across all methods. For VR-GS, we set the XPBD iteration per substep to 1, as the small Δt_{step} sufficiently resolves the dynamics. As depicted in Figure 6 and the inset table, VR-GS not only matches the visual quality of PhysGaussian but also outperforms PAC-NeRF in clarity and realism. Crucially, our XPBD-based simulation framework allows for significantly faster simulations, making VR-GS ideal for real-time, physics-aware interactions in VR.

6.2 VR Demos

Our VR-GS system’s capability to replicate real-world scenarios is showcased through several representative demos. These demos, employing GS and our dynamic simulation model, illustrate the system’s interactive and immersive qualities. Detailed simulation



Fig. 6. **Visual Quality Comparison.** Our method synthesizes competitive visual results compared to PhysGaussian [60] and significantly outperforms PAC-NeRF [25].

Table 1. **Parameters and Timings of Demos in Section 6.2.**

| Example | #Gaussians | #Verts. | #Iter* | CD* | FPS |
|----------------------------|------------|---------|--------|-----|-------|
| (Figure 7) Fox | 304,875 | 28,205 | 1 | 10 | 161.2 |
| (Figure 7) Bear | 2,525,891 | 60,590 | 10 | 10 | 36.3 |
| (Figure 7) Horse | 1,295,223 | 10,611 | 5 | 10 | 115.4 |
| (Figure 9) Ring Toss | 956,116 | 17,513 | 20 | 10 | 39.0 |
| (Figure 10) Toy Collection | 2,555,482 | 46,810 | 5 | 5 | 19.3 |
| (Figure 4) Box Moving | 1,769,412 | 1,434 | 10 | 1 | 73.8 |
| (Figure 1) Animal Crossing | 1,031,191 | 44,969 | 15 | 10 | 33.5 |

* #Iter: XPBD iteration count; CD: collision detection per step.

setups and a timing breakdown for these demos are provided in Table 1 and Figure 8.

Fox, Bear, and Horse Manipulation. VR-GS empowers users to edit 3D Gaussian kernels in a user-friendly manner, utilizing our XPBD-based physics engine for dynamic manipulation. We demonstrate this through three examples: a fox, a bear, and a horse, reconstructed from the Instant-NGP dataset [36], the Instruct-NeRF2NeRF [13], and the Tanks and Temples dataset [18], respectively. Each object’s Gaussian kernels are segmented from their scenes and converted into tetrahedron meshes, allowing for physics-based post-manipulation. The interactions, as depicted in Figure 7, exhibit lively responses to user inputs within the 3D environment.

Ring Toss. In this scenario, we demonstrate the system’s ability to seamlessly integrate new virtual objects into pre-existing scenes. A room scene, reconstructed from our collected real-world data, and a virtual ring, modeled in Blender, are used to create a ring toss game. The dining table and objects on it serve as collision boundaries for the ring. This interaction, shown in Figure 9, highlights VR-GS’s capacity to blend reconstructed and virtual objects in a unified framework, creating an immersive VR experience.

Toy Collection. To further assess the system’s efficiency and efficacy with multiple interactive objects, we reconstructed a living room scene and a set of plush toys, the latter partly synthesized using LucidDreamer [26]. This setup, illustrated in Figure 10, allows users to realistically interact with the toys, showcasing VR-GS’s ability to handle complex scenarios involving a mix of 3D GS objects derived from real and synthesized environments.



Fig. 7. **Fox, Bear, and Horse.** Our proposed VR-GS allows users to manipulate 3D GS at a real-time rate with physically plausible response.

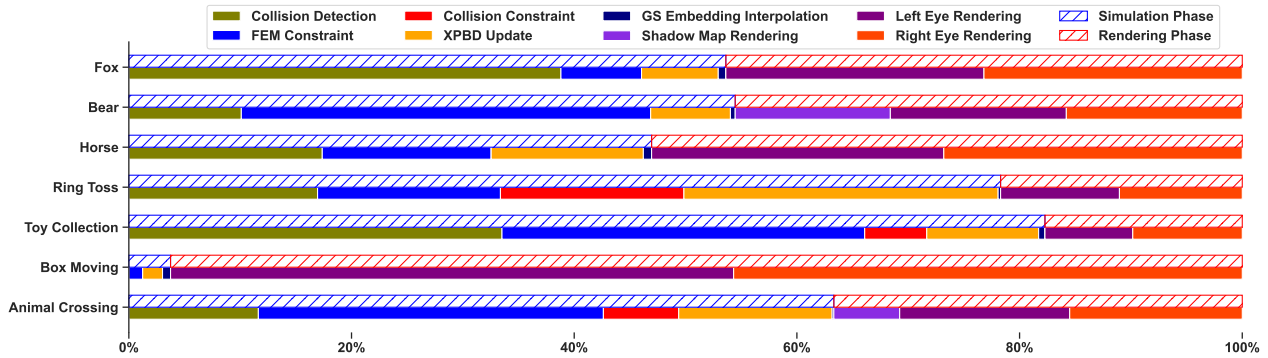


Fig. 8. **Timing Breakdown of Demos in Section 6.2.**

Animal Crossing. The *Animal Crossing* background scene is the same as the *Ring Toss* scene. All four animal models sitting on chairs are reconstructed from *Toy Collection*. VR-GS permitted free deformation of the animal models, enabling users to freely interact with them. As demonstrated in Figure 1, this setup leveraged our sophisticated generative dynamics, resulting in objects reacting to impacts in a manner that closely mimics real-world physics.

7 USER STUDY

We conducted a user study with 10 participants: 2 professionals (P1–P2) with 5 and 7 years of experience in 3D VFX software (including Houdini and Blender), and 8 novices (P3–P10), with P2 also having 2 years of VR experience. Our study used the hardware specified in the experimental section and included the Fox, Ring Toss, and Toy Collection demos. Participants received a 10-minute video tutorial on our system before completing two tasks. Post-task, they answered a questionnaire covering usability (System Usability Scale



Fig. 9. **Ring Toss.** Utilizing our VR-GS system, participants can engage in an interactive ring toss game simulated within authentic environments.



Fig. 10. **Toy Collection.** We place all the toys on the sofa, and then move them into the basket. After shaking the basket, all the toys fly out in a realistic way.

[1]) and subjective feedback on individual (M1-M5: object manipulation, inpainted scene, illumination, realistic dynamics, physics-based placement) and overall system features (M6-M9: easiness to use, latency satisfaction, functionality, overall satisfaction), as shown in Section 7.2. Additionally, we conducted a 20-minute semi-structured interview for more in-depth feedback.

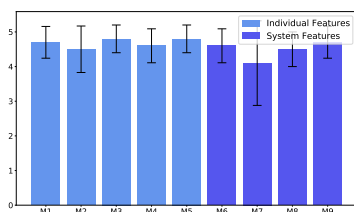
7.1 Tasks

Task 1: Goal-directed (30 minutes). The participants were required to pet a fox (Figure 7) and complete two VR games developed from our system, including ring toss (Figure 9) and toy collection (Figure 10). Each subtask is a 10-minute session. More specifically, in the ring toss task, users are required to throw rings over the objects on the table, and in the toy collection task, users are required to collect messy toys from the living room into a basket. Task 1 has been specifically designed to enable users to interact comprehensively with the primary features of our system. The order of the three subtasks was counterbalanced by a Latin square design to minimize possible learning effects.

Task 2: Open-ended (30 minutes). The participants are asked to edit the scene and generate dynamics freely with our prototype system, which includes geometry-based editing, physics-based editing, transform, rotation, duplicating, undoing, rescaling, etc.

7.2 Results and Discussion

The inset figure summarizes the subjective feedback about the individual features and system features including easiness to



use, latency satisfaction, system functionality, and overall satisfaction. Overall, our system has received positive opinions. Among various features, users spoke highly of the placement of virtual content. Transforming objects without physics rules resulted in floating objects, while in our system, all virtual content placements, such as putting toys onto a sofa, are followed by physics rules and are consistent with the user's understanding and convention. P7 commented, "I love this a lot. I have a dog. Petting the fox is really like what I did to my dog at home. I felt so real. Moreover, the placement of the toy is awesome. After they all fell to the basket, the basket even shook for a while" The VR-GS system's realistic lighting and physics-based dynamics create an immersive experience. As a professional user, P2 spoke highly of high-fidelity generative dynamics and illumination. "Those motions of virtual content are just like what I see in the physical world. I can't wait to take photos of my own house and then put them in VR with my video game character." Users rated the system highly on ease of use (4.6/5) and overall satisfaction (4.8/5). With a System Usability Scale (SUS) score of 83.5, VR-GS is classified as 'excellent' according to [1].

8 CONCLUSION AND FUTURE WORK

This paper has presented VR-GS, a physical dynamics-aware interactive Gaussian Splatting system in VR, particularly first addressing the challenge of editing real-time high-fidelity virtual content. By leveraging the advancements in Gaussian Splatting, VR-GS bridges the quality gap traditionally observed between machine-generated and manually created 3D content. Our system not only enhances the reality and immersion via physically-based dynamics, but also provides fine-grained interaction and manipulation controllability.

Although all the study participants appreciated the efficiency and effectiveness of our proposed VR-GS, it still remains to be improved. Firstly, rendering high-fidelity Gaussian kernels in VR is computationally demanding. As a result, rendering generative dynamics in a large scene with 2K resolution might lead to potential latency issues in our system. Secondly, we will extend our system to fluid simulation as a future work, a significant aspect of simulation and editing in realistic scenarios. In future iterations, we aim to incorporate a broader range of materials, such as fluid and cloth, to enhance the system's capabilities.

REFERENCES

- [1] Aaron Bangor, Philip Kortum, and James Miller. 2009. Determining what individual SUS scores mean: Adding an adjective rating scale. *Journal of usability studies* 4, 3 (2009), 114–123.
- [2] Chong Bao, Yinda Zhang, Bangbang Yang, Tianxing Fan, Zesong Yang, Hujun Bao, Guofeng Zhang, and Zhaopeng Cui. 2023. Sine: Semantic-driven image-based nerf editing with prior-guided editing field. In *Proceedings of the IEEE/CVF Conference on Computer Vision and Pattern Recognition*. 20919–20929.
- [3] Jianchuan Chen, Ying Zhang, Di Kang, Xuefei Zhe, Linchao Bao, Xu Jia, and Huchuan Lu. 2021. Animatable neural radiance fields from monocular rgb videos. *arXiv preprint arXiv:2106.13629* (2021).
- [4] Yiwen Chen, Zilong Chen, Chi Zhang, Feng Wang, Xiaofeng Yang, Yikai Wang, Zhongang Cai, Lei Yang, Huaping Liu, and Guosheng Lin. 2023. Gaussianeditor: Swift and controllable 3d editing with gaussian splatting. *arXiv preprint arXiv:2311.14521* (2023).
- [5] Ho Kei Cheng, Seoung Wug Oh, Brian Price, Joon-Young Lee, and Alexander Schwing. 2023. Putting the Object Back into Video Object Segmentation. *arXiv preprint arXiv:2310.12982* (2023).
- [6] Nianchen Deng, Zhenyi He, Jiannan Ye, Budmonde Duinkharjav, Praneeth Chakravarthula, Xubo Yang, and Qi Sun. 2022. Fov-nerf: Foveated neural radiance fields for virtual reality. *IEEE Transactions on Visualization and Computer Graphics* 28, 11 (2022), 3854–3864.
- [7] Bardienus P Duisterhof, Zhao Mandi, Yunchao Yao, Jia-Wei Liu, Mike Zheng Shou, Shuran Song, and Jeffrey Ichnowski. 2023. MD-Splatting: Learning Metric Deformation from 4D Gaussians in Highly Deformable Scenes. *arXiv preprint arXiv:2312.00583* (2023).
- [8] Jiemin Fang, Junjie Wang, Xiaopeng Zhang, Lingxi Xie, and Qi Tian. 2023. Gaussianeditor: Editing 3d gaussians delicately with text instructions. *arXiv preprint arXiv:2311.16037* (2023).
- [9] Yutao Feng, Yintong Shang, Xuan Li, Tianjia Shao, Chenfanfu Jiang, and Yin Yang. 2023. PIE-NeRF: Physics-based Interactive Elastodynamics with NeRF. *arXiv preprint arXiv:2311.13099* (2023).
- [10] Joseph L Gabbard, Deborah Hix, and J Edward Swan. 1999. User-centered design and evaluation of virtual environments. *IEEE computer Graphics and Applications* 19, 6 (1999), 51–59.
- [11] Lin Gao, Jia-Mu Sun, Kaichun Mo, Yu-Kun Lai, Leonidas J Guibas, and Jie Yang. 2023. SceneHGN: Hierarchical Graph Networks for 3D Indoor Scene Generation with Fine-Grained Geometry. *IEEE Transactions on Pattern Analysis and Machine Intelligence* (2023).
- [12] Kelly S Hale and Kay M Stanney. 2014. *Handbook of virtual environments: Design, implementation, and applications*. CRC Press.
- [13] Ayaan Haque, Matthew Tancik, Alexei A Efros, Aleksander Holynski, and Angjoo Kanazawa. 2023. Instruct-nerf2nerf: Editing 3d scenes with instructions. *arXiv preprint arXiv:2303.12789*.
- [14] Yi-Hua Huang, Yan-Pei Cao, Yu-Kun Lai, Ying Shan, and Lin Gao. 2023. NeRFtexture: Texture synthesis with neural radiance fields. In *ACM SIGGRAPH 2023 Conference Proceedings*. 1–10.
- [15] Yi-Hua Huang, Yang-Tian Sun, Ziyi Yang, Xiaoyang Lyu, Yan-Pei Cao, and Xiaojuan Qi. 2023. SC-GS: Sparse-Controlled Gaussian Splatting for Editable Dynamic Scenes. *arXiv preprint arXiv:2312.14937* (2023).
- [16] Roy S Kalawsky. 1999. VRUSE—a computerised diagnostic tool: for usability evaluation of virtual/synthetic environment systems. *Applied ergonomics* 30, 1 (1999), 11–25.
- [17] Bernhard Kerbl, Georgios Kopanas, Thomas Leimkühler, and George Drettakis. 2023. 3D Gaussian Splatting for Real-Time Radiance Field Rendering. *ACM Transactions on Graphics* 42, 4 (2023).
- [18] Arno Knapitsch, Jaesik Park, Qian-Yi Zhou, and Vladlen Koltun. 2017. Tanks and temples: Benchmarking large-scale scene reconstruction. *ACM Transactions on Graphics (ToG)* 36, 4, 1–13.
- [19] Chaojian Li, Sixu Li, Yang Zhao, Wenbo Zhu, and Yingyan Lin. 2022. RT-NeRF: Real-Time On-Device Neural Radiance Fields Towards Immersive AR/VR Rendering. In *Proceedings of the 41st IEEE/ACM International Conference on Computer-Aided Design*. 1–9.
- [20] Ke Li, Tim Rolf, Reinhard Bacher, and Frank Steinicke. 2023. RealityGit: Cross Reality Version Control of R&D Optical Workbench. In *2023 IEEE International Symposium on Mixed and Augmented Reality Adjunct (ISMAR-Adjunct)*. IEEE, 807–808.
- [21] Ke Li, Tim Rolf, Susanne Schmidt, Reinhard Bacher, Simone Frintrop, Wim Leemans, and Frank Steinicke. 2022. Immersive Neural Graphics Primitives. *arXiv preprint arXiv:2211.13494* (2022).
- [22] Ke Li, Tim Rolf, Susanne Schmidt, Reinhard Bacher, Wim Leemans, and Frank Steinicke. 2023. Interacting with Neural Radiance Fields in Immersive Virtual Reality. In *Extended Abstracts of the 2023 CHI Conference on Human Factors in Computing Systems*. 1–4.
- [23] Ke Li, Susanne Schmidt, Tim Rolf, Reinhard Bacher, Wim Leemans, and Frank Steinicke. 2023. Magic nerf lens: Interactive fusion of neural radiance fields for virtual facility inspection. *arXiv preprint arXiv:2307.09860* (2023).
- [24] Shaou Li and Ye Pan. 2023. Interactive Geometry Editing of Neural Radiance Fields. *arXiv preprint arXiv:2303.11537* (2023).
- [25] Xuan Li, Yi-Ling Qiao, Peter Yichen Chen, Krishna Murthy Jatavallabhula, Ming Lin, Chenfanfu Jiang, and Chuang Gan. 2023. PAC-nerf: Physics augmented continuum neural radiance fields for geometry-agnostic system identification. *arXiv preprint arXiv:2303.05512* (2023).
- [26] Yixun Liang, Xin Yang, Jiantao Lin, Haodong Li, Xiaogang Xu, and Yingcong Chen. 2023. LucidDreamer: Towards High-Fidelity Text-to-3D Generation via Interval Score Matching. *arXiv preprint arXiv:2311.11284* (2023).
- [27] Gao Lin, Liu Feng-Lin, Chen Shu-Yu, Jiang Kaiwen, Li Chunpeng, Yukun Lai, and Fu Hongbo. 2023. SketchFaceNeRF: Sketch-based facial generation and editing in neural radiance fields. *ACM Transactions on Graphics* (2023).
- [28] David B Lindell, Julien NP Martel, and Gordon Wetzstein. 2021. Autoit: Automatic integration for fast neural volume rendering. In *Proceedings of the IEEE/CVF Conference on Computer Vision and Pattern Recognition*. 14556–14565.
- [29] Lingjie Liu, Jiatao Gu, Kyaw Zaw Lin, Tat-Seng Chua, and Christian Theobalt. 2020. Neural sparse voxel fields. *Advances in Neural Information Processing Systems* 33 (2020), 15651–15663.
- [30] Stephen Lombardi, Tomas Simon, Gabriel Schwartz, Michael Zollhoefer, Yaser Sheikh, and Jason Saragih. 2021. Mixture of volumetric primitives for efficient neural rendering. *ACM Transactions on Graphics (ToG)* 40, 4 (2021), 1–13.
- [31] William E. Lorensen and Harvey E. Cline. 1987. Marching cubes: A high resolution 3D surface construction algorithm. *SIGGRAPH Comput. Graph.* 21, 4 (aug 1987), 163–169.
- [32] Miles Macklin, Matthias Müller, and Nuttapon Chentanez. 2016. XPBD: position-based simulation of compliant constrained dynamics. In *Proceedings of the 9th International Conference on Motion in Games (Burlingame, California) (MIG '16)*. Association for Computing Machinery, New York, NY, USA, 49–54.
- [33] Xiaoxu Meng, Weikai Chen, and Bo Yang. 2023. NeAT: Learning Neural Implicit Surfaces with Arbitrary Topologies from Multi-view Images. In *Proceedings of the IEEE/CVF Conference on Computer Vision and Pattern Recognition*. 248–258.
- [34] Ben Mildenhall, Pratul P Srinivasan, Matthew Tancik, Jonathan T Barron, Ravi Ramamoorthi, and Ren Ng. 2021. Nerf: Representing scenes as neural radiance fields for view synthesis. *Commun. ACM* 65, 1 (2021), 99–106.
- [35] Matthias Müller, Nuttapon Chentanez, and Miles Macklin. 2016. Simulating visual geometry. In *Proceedings of the 9th International Conference on Motion in Games (Burlingame, California) (MIG '16)*. Association for Computing Machinery, New York, NY, USA, 31–38.
- [36] Thomas Müller, Alex Evans, Christoph Schied, and Alexander Keller. 2022. Instant neural graphics primitives with a multiresolution hash encoding. *ACM Transactions on Graphics (ToG)* 41, 4 (2022), 1–15.
- [37] Ken Museth. 2013. VDB: High-resolution sparse volumes with dynamic topology. *ACM Trans. Graph.* 32, 3, Article 27 (jul 2013), 22 pages.
- [38] Michael Niemeyer and Andreas Geiger. 2021. Campari: Camera-aware decomposed generative neural radiance fields. In *2021 International Conference on 3D Vision (3DV)*. IEEE, 951–961.
- [39] Michael Oechsle, Songyou Peng, and Andreas Geiger. 2021. Unisurf: Unifying neural implicit surfaces and radiance fields for multi-view reconstruction. In *Proceedings of the IEEE/CVF International Conference on Computer Vision*. 5589–5599.
- [40] J. Pantaleoni and D. Luebke. 2010. HLBVH: hierarchical LBVH construction for real-time ray tracing of dynamic geometry. In *Proceedings of the Conference on High Performance Graphics (Saarbrücken, Germany) (HPG '10)*. Eurographics Association, Goslar, DEU, 87–95.
- [41] Keunhong Park, Utkarsh Sinha, Jonathan T Barron, Sofien Bouaziz, Dan B Goldman, Steven M Seitz, and Ricardo Martin-Brualla. 2021. Nerfies: Deformable neural radiance fields. In *Proceedings of the IEEE/CVF International Conference on Computer Vision*. 5865–5874.

- [42] Sida Peng, Junting Dong, Qianqian Wang, Shangzhan Zhang, Qing Shuai, Xiaowei Zhou, and Hujun Bao. 2021. Animatable neural radiance fields for modeling dynamic human bodies. In *Proceedings of the IEEE/CVF International Conference on Computer Vision*. 14314–14323.
- [43] Albert Pumarola, Enric Corona, Gerard Pons-Moll, and Francesc Moreno-Noguer. 2021. D-nerf: Neural radiance fields for dynamic scenes. In *Proceedings of the IEEE/CVF Conference on Computer Vision and Pattern Recognition*. 10318–10327.
- [44] Charles R Qi, Hao Su, Kaichun Mo, and Leonidas J Guibas. 2017. Pointnet: Deep learning on point sets for 3d classification and segmentation. In *Proceedings of the IEEE conference on computer vision and pattern recognition*. 652–660.
- [45] Yi-Ling Qiao, Alexander Gao, Yiran Xu, Yue Feng, Jia-Bin Huang, and Ming C Lin. 2023. Dynamic mesh-aware radiance fields. In *Proceedings of the IEEE/CVF International Conference on Computer Vision*. 385–396.
- [46] Daniel Rebain, Wei Jiang, Soroosh Yazdani, Ke Li, Kwang Moo Yi, and Andrea Tagliasacchi. 2021. Derf: Decomposed radiance fields. In *Proceedings of the IEEE/CVF Conference on Computer Vision and Pattern Recognition*. 14153–14161.
- [47] Tim Rolf, Susanne Schmidt, Ke Li, Frank Steinicke, and Simone Frintrop. 2023. VRS-NeRF: Accelerating Neural Radiance Field Rendering with Variable Rate Shading. In *2023 IEEE International Symposium on Mixed and Augmented Reality (ISMAR)*. IEEE, 243–252.
- [48] Hang Si. 2015. TetGen, a Delaunay-Based Quality Tetrahedral Mesh Generator. *ACM Trans. Math. Softw.* 41, 2, Article 11 (feb 2015), 36 pages.
- [49] Liangchen Song, Anpei Chen, Zhong Li, Zhang Chen, Lele Chen, Junsong Yuan, Yi Xu, and Andreas Geiger. 2023. Nerfplayer: A streamable dynamic scene representation with decomposed neural radiance fields. *IEEE Transactions on Visualization and Computer Graphics* 29, 5 (2023), 2732–2742.
- [50] Olga Sorkine and Daniel Cohen-Or. 2004. Least-squares meshes. In *Proceedings Shape Modeling Applications, 2004*. IEEE, 191–199.
- [51] Kay M Stanney, Mansooreh Mollaghasemi, Leah Reeves, Robert Breaux, and David A Graeber. 2003. Usability engineering of virtual environments (VEs): identifying multiple criteria that drive effective VE system design. *International Journal of Human-Computer Studies* 58, 4 (2003), 447–481.
- [52] Jia-Mu Sun, Tong Wu, Yong-Liang Yang, Yu-Kun Lai, and Lin Gao. 2023. SOL-NeRF: Sunlight modeling for outdoor scene decomposition and relighting. In *SIGGRAPH Asia 2023 Conference Papers*. 1–11.
- [53] Alistair G Sutcliffe, Charalambos Poullis, Andreas Gregoriades, Irene Katsouri, Aimilia Tzanavari, and Kyriakos Herakleous. 2019. Reflecting on the design process for virtual reality applications. *International Journal of Human-Computer Interaction* 35, 2 (2019), 168–179.
- [54] Roman Suvorov, Elizaveta Logacheva, Anton Mashikhin, Anastasia Remizova, Arsenii Ashukha, Aleksei Silvestrov, Naejin Kong, Harshith Goka, Kiwoong Park, and Victor Lempitsky. 2022. Resolution-robust large mask inpainting with fourier convolutions. In *Proceedings of the IEEE/CVF winter conference on applications of computer vision*. 2149–2159.
- [55] Haithem Turki, Vasu Agrawal, Samuel Rota Bulò, Lorenzo Porzi, Peter Kotschieder, Deva Ramanan, Michael Zollhöfer, and Christian Richardt. 2023. HybridNeRF: Efficient Neural Rendering via Adaptive Volumetric Surfaces. *arXiv preprint arXiv:2312.03160* (2023).
- [56] Can Wang, Ruixiang Jiang, Menglei Chai, Mingming He, Dongdong Chen, and Jing Liao. 2023. Nerf-art: Text-driven neural radiance fields stylization. *IEEE Transactions on Visualization and Computer Graphics* (2023).
- [57] Peng Wang, Lingjie Liu, Yuan Liu, Christian Theobalt, Taku Komura, and Wenping Wang. 2021. Neus: Learning neural implicit surfaces by volume rendering for multi-view reconstruction. *arXiv preprint arXiv:2106.10689* (2021).
- [58] L.R. Wanger, J.A. Ferwerda, and D.P. Greenberg. 1992. Perceiving spatial relationships in computer-generated images. *IEEE Computer Graphics and Applications* 12, 3, 44–58.
- [59] Tong Wu, Jia-Mu Sun, Yu-Kun Lai, and Lin Gao. 2023. De-nerf: Decoupled neural radiance fields for view-consistent appearance editing and high-frequency environmental relighting. In *ACM SIGGRAPH 2023 conference proceedings*. 1–11.
- [60] Tianyi Xie, Zeshun Zong, Yuxin Qiu, Xuan Li, Yutao Feng, Yin Yang, and Chenfanfu Jiang. 2023. Physgaussian: Physics-integrated 3d gaussians for generative dynamics. *arXiv preprint arXiv:2311.12198* (2023).
- [61] Yiheng Xie, Towaki Takikawa, Shunsuke Saito, Or Litany, Shiqin Yan, Numair Khan, Federico Tombari, James Tompkin, Vincent Sitzmann, and Srinath Sridhar. 2022. Neural fields in visual computing and beyond. In *Computer Graphics Forum*, Vol. 41. Wiley Online Library, 641–676.
- [62] Linning Xu, Vasu Agrawal, William Laney, Tony Garcia, Aayush Bansal, Changil Kim, Samuel Rota Bulò, Lorenzo Porzi, Peter Kotschieder, Aljaž Božič, et al. 2023. VR-NeRF: High-fidelity virtualized walkable spaces. In *SIGGRAPH Asia 2023 Conference Papers*. 1–12.
- [63] Yuelang Xu, Benwang Chen, Zhe Li, Hongwen Zhang, Lizhen Wang, Zerong Zheng, and Yebin Liu. 2023. Gaussian Head Avatar: Ultra High-fidelity Head Avatar via Dynamic Gaussians. *arXiv preprint arXiv:2312.03029* (2023).
- [64] Zeyu Yang, Hongye Yang, Zijie Pan, Xiatian Zhu, and Li Zhang. 2023. Real-time photorealistic dynamic scene representation and rendering with 4d gaussian splatting. *arXiv preprint arXiv:2310.10642* (2023).
- [65] Lior Yariv, Jiatao Gu, Yoni Kasten, and Yaron Lipman. 2021. Volume rendering of neural implicit surfaces. *Advances in Neural Information Processing Systems* 34 (2021), 4805–4815.
- [66] Mingqiao Ye, Martin Danelljan, Fisher Yu, and Lei Ke. 2023. Gaussian grouping: Segment and edit anything in 3d scenes. *arXiv preprint arXiv:2312.00732* (2023).
- [67] Yongning Zhu and Robert Bridson. 2005. Animating sand as a fluid. *ACM Transactions on Graphics (TOG)* 24, 3 (2005), 965–972.
- [68] Wojciech Zielonka, Timur Bagautdinov, Shunsuke Saito, Michael Zollhöfer, Justus Thies, and Javier Romero. 2023. Drivable 3d gaussian avatars. *arXiv preprint arXiv:2311.08581* (2023).